Materials Advances

ROYAL SOCIETY OF CHEMISTRY

PAPER

View Article Online
View Journal | View Issue

Open Access Article. Published on 30 May 2025. Downloaded on 11/9/2025 1:50:11 PM.
This article is licensed under a Creative Commons Attribution-NonCommercial 3.0 Unported Licence.

Check for updates

Cite this: *Mater. Adv.*, 2025, 6, 4325

Highly photoluminescent carbon dots: a multifunctional platform for pH sensing, nano thermometry, and mercury(II) detection

Mouna Fhoula,[a] Ikhlas Kchaou,[a] Christian Hernández-Álvarez,[d] Mohamed Dammak,*[a] Sami Boufi[b] and Inocencio R. Martín[c]

Received 20th March 2025,
Accepted 25th May 2025

DOI: 10.1039/d5ma00250h

rsc.li/materials-advances

Carbon dots (CDs), a class of heavy-metal-free fluorescent nanomaterials, have attracted significant attention due to their excellent optical properties, chemical stability, low toxicity, and biocompatibility. In this study, highly photoluminescent N-CDs with small sizes and exceptional quantum yields (up to 90%) were successfully synthesized using citric acid and tri-(2-aminoethyl)amine *via* a hydrothermal method. The synthesized N-CDs exhibit a single emission band at 450 nm under 380 nm excitation and dual emission bands at 460 nm and 581 nm under 258 nm excitation. Notably, their fluorescence emission spectra display strong temperature dependence and pH-responsive behaviour, rendering them highly versatile as nano thermometric devices. Specifically, their emission intensity demonstrates remarkable sensitivity across the temperature range of 298–343 K, enabling precise thermal measurements. Moreover, these N-CDs function effectively as pH sensors, further expanding their utility. Additionally, the fluorescence of the N-CDs is rapidly and selectively enhanced in the presence of Hg^{2+} ions at room temperature, without requiring any surface modification. This enhancement exhibits a linear relationship within the concentration range of 0–10 μM, with a detection limit as low as 0.46 μM. These findings highlight the multifunctional nature of the synthesized N-CDs, which hold great promise for applications in pH sensing, nano thermometry, and the specific detection of mercury ions.

1. Introduction

Carbon dots (CDs), as a highly promising carbon-based nanomaterial, have gained significant attention due to their exceptional properties, including good biocompatibility, high fluorescence stability, high quantum yield (QY), low toxicity, excellent aqueous dispersibility, eco-friendliness, facile preparation and wide possibilities of functionalization.[1–5] Recently, CDs have been widely utilized in diverse applications, including drug delivery, light-emitting diode (LED) materials, bioimaging, optical detection probes, biosensors, and medical imaging.[6–16] With sizes typically below 10 nm, CDs can be readily synthesized through various methods, such as electrochemical oxidation, microwave treatment, ultrasonic processing, laser irradiation, strong acid oxidation, solvothermal, and hydrothermal methods, the latter being particularly simple and efficient for producing fluorescent CDs using wide arrays of organic affordable precursors.[17–24]

However, the synthesis of CDs with high fluorescence intensity and tunable emission properties remains a challenging task for researchers in the field of nanomaterials. Notably, the photoluminescence (PL) properties of CDs are highly sensitive to their environment, making them ideal candidates for sensing applications. A broad range of ionic and molecular species can interact with the surface functional groups of CDs, inducing changes in their PL emission. Importantly, the PL properties of CDs are extremely responsive to their surrounding environment, which makes them valuable tools for sensing applications. Various ionic and molecular species can bind to or interact with the surface groups of CDs, causing alterations in their PL emission.[25,26] Consequently, CDs have been effectively employed as fluorescent agents in sensing applications for detecting a variety of analytes, such as heavy metal ions, temperature, pH, and mercury ions.[27–33] Their tunable optical properties, combined with high quantum yield and sensitivity, enable effective and precise detection in these applications.

Among the various strategies for tuning the properties of carbon dots (CDs), the pH-dependent photoluminescence (PL)

[a] *Laboratoire de Physique Appliquée, Faculté des Sciences de Sfax, Département de Physique, Université de Sfax, Sfax, B.P. 3000, Tunisia. E-mail: madidammak@yahoo.fr, mohamed.dammak@fss.usf.tn*
[b] *University of Sfax, LMSE, Faculty of Science, BP 802, 3018 Sfax, Tunisia*
[c] *Universidad de La Laguna, Departamento de Física, MALTA-Consolider Team and IMN. Apdo. Correos 456, E-38206 San Cristóbal de La Laguna, Santa Cruz de Tenerife, Spain*
[d] *Adam Mickiewicz University, Faculty of Chemistry, Uniwersytetu Poznańskiego 8, 61-614 Poznań, Poland*

© 2025 The Author(s). Published by the Royal Society of Chemistry

Open Access Article. Published on 30 May 2025. Downloaded on 11/9/2025 1:50:11 PM.
This article is licensed under a Creative Commons Attribution-NonCommercial 3.0 Unported Licence.

behaviour has emerged as a key area of research. To date, numerous studies have reported successful examples of CDs with pH-responsive tuneable properties.[32,34–37] The underlying mechanism in these systems typically involves luminescence enhancement or quenching of a single emission peak under varying pH conditions. However, this approach can be influenced by several interfering factors, such as fluctuations in the excitation source, environmental variations, and changes in probe concentration. To address these limitations, researchers have developed CDs with intrinsic pH-sensitive dual-emission characteristics, enabling the creation of label-free ratiometric fluorescence pH nanoprobes.[38–40] Moreover, CDs have demonstrated significant potential for detecting heavy metal ions due to their unique photoluminescence properties and high selectivity toward specific metal ions, such as Co^{2+},[41,42] Mg^{2+},[43] Fe^{3+},[28] Pb^{2+}, Cu^{2+},[44] Ag^{+},[45] and Hg^{2+}.[33] Among these cations, CDs have shown exceptional performance in the selective detection of mercury(II) (Hg^{2+}), alongside good water dispersibility. Hg(II) is one of the most hazardous heavy metal ions, capable of causing severe health issues even at extremely low concentrations.[46] Recently, several fluorescent probes based on CDs have been developed for the selective detection of Hg(II) ions. Notably, the majority of these methods rely on fluorescence quenching ("turn-off") mechanisms,[33,45] while fewer reports focus on fluorescence enhancement ("turn-on") approaches.[47,48] Generally, "turn-on" mechanisms are preferred over "turn-off" mechanisms due to their higher selectivity and reduced likelihood of false positives.[49] Consequently, there is considerable interest in developing new detection techniques based on the fluorescence-enhancement mechanism.

Despite recent progress in carbon dot (CD) research, existing systems often suffer from compromised functionality (*e.g.*, single-application focus), moderate quantum yields (<60%), or reliance on surface modifications to achieve selective ion detection. In this study, we address these limitations by synthesizing nitrogen-doped carbon dots (N-CDs) *via* a simple hydrothermal method using citric acid and tri-(2-aminoethyl)-amine (TREN). Unlike previous CD platforms, our N-CDs achieve three key advancements: Unprecedented quantum yield (90%), surpassing most reported CDs; intrinsic dual-emission behavior (450 nm under 380 nm excitation; 460/581 nm under 258 nm excitation) without requiring external dopants; and multifunctionality enabling Hg^{2+} detection, pH sensing, and temperature-responsive PL behavior within a single system. Remarkably, Hg^{2+} detection is achieved *via* a fluorescence-enhancement mechanism at ambient conditions, eliminating the need for surface modification a critical advantage over conventional CDs requiring complex functionalization. Furthermore, the temperature-dependent PL (298–343 K) and pH-responsive behavior demonstrate precision comparable to specialized nanosensors. This work represents the first demonstration of CDs combining such high efficiency, dual-emission versatility, and triple functionality, offering a transformative platform for environmental monitoring and multimodal analytical applications.

2. Experimental

2.1. Materials

Citric acid (CA), tri-(2-aminoethyl)amine (TREN), $MnCl_2$, $NiCl_2$, $CdCl_2$, $HgCl_2$, $MgCl_2$, $ZnCl_2$, $CoSO_4{\cdot}H_2O$, $NaNO_3$, $Ca(NO_3)_2$, $Ba(NO_3)_2$, $Bi(NO_3)_3$, and NaOH were all procured from Sigma-Aldrich. All chemicals were used as received without further purification. Deionized (DI) water was employed for the preparation of all solutions.

2.2. Preparation of pure N-CDs

The carbon dots (CDs) were synthesized using the hydrothermal method with citric acid (CA) and tri-(2-aminoethyl)amine (TREN) as precursors (Fig. 1). Initially, 1 g of CA and 0.4 g of

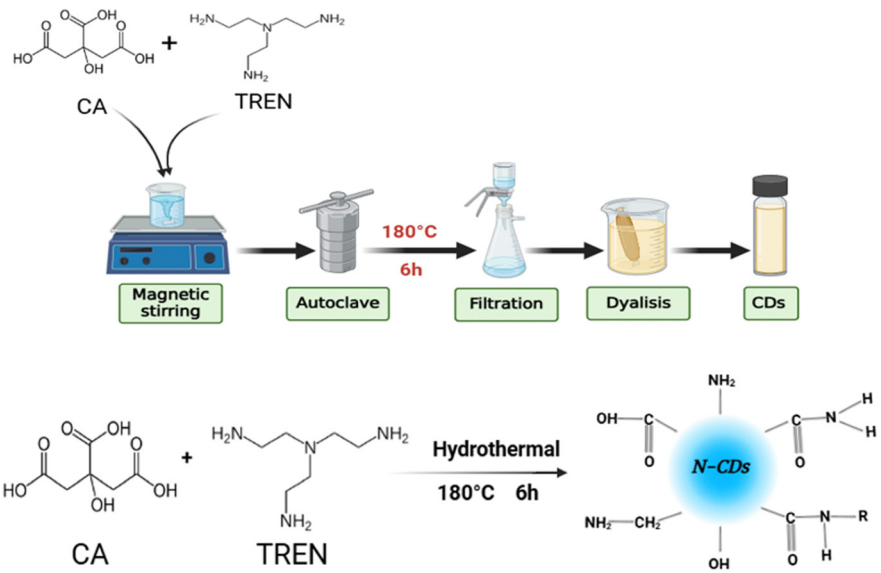

Fig. 1 Schematic representation of the hydrothermal method for the synthesis of N-CDs.

 © 2025 The Author(s). Published by the Royal Society of Chemistry

Open Access Article. Published on 30 May 2025. Downloaded on 11/9/2025 1:50:11 PM.
This article is licensed under a Creative Commons Attribution-NonCommercial 3.0 Unported Licence.

TREN were accurately weighed and dissolved in 25 mL of deionized (DI) water in a beaker. The solution was stirred vigorously at room temperature for 30 minutes to ensure complete homogenization. Subsequently, the resulting mixture was transferred to a Teflon-lined stainless-steel autoclave and heated in a furnace at 180 °C for 6 hours. After the reaction, the autoclave was allowed to cool naturally to room temperature. The resulting brown solution was then filtered through a 0.22 μm filter membrane to remove any insoluble impurities. To further purify the CDs, the filtrate was dialyzed against deionized (DI) water for 3 days using a dialysis bag with a molecular weight cut-off (MWCO) of 1000 Da, ensuring the removal of small molecular weight by-products.

The purified solution inside the dialysis bag was collected and either stored at 4 °C for subsequent use in liquid form, or freeze-dried for 24 hours to obtain solid-state N-CDs when required. This process yielded high-quality nitrogen-doped carbon dots (N-CDs).

2.3. pH adjustment of N-CDs aqueous solution

The pH of the N-CDs solution was adjusted by adding 2 M NaOH to vary it within the range of 4 to 12. Fluorescence spectra were subsequently recorded at each pH level to investigate the effect of pH on the photoluminescence properties of the N-CDs.

2.4. Detection of Hg(II) ions using CDs

The detection of Hg(II) ions was carried out at room temperature. Initially, carbon dots (CDs) were dispersed in deionized (DI) water to prepare a stock solution with a concentration of 1 mg mL^{-1}. To evaluate the sensitivity of N-CDs toward Hg(II) ions, 2 mL of aqueous Hg(II) solutions at concentrations ranging from 0 to 250 μM were added to 2 mL of the N-CDs solution. The mixtures were then stirred for 10 minutes to ensure thorough interaction between the CDs and Hg(II) ions. Fluorescence spectra were subsequently recorded using an excitation wavelength of 380 nm.

A similar procedure was employed for the detection of other metal ions, including Co^{2+}, Mg^{2+}, Ba^{2+}, Ca^{2+}, Zn^{2+}, Cd^{2+}, Mn^{2+}, Ni^{2+}, Na^{+}, and Bi^{3+}, all at a uniform concentration of 250 μM. This allowed for a comparative analysis of the selectivity of the N-CDs toward Hg(II) ions relative to other common metal ions.

2.5. Characterization

•Transmission electron microscopy (TEM): this technique was used to observe the morphology and estimate the size of the N-CDs at the nanoscale. TEM measurements were made on a HITACHI H-8100 electron microscope with an accelerating voltage of 200 kV.

•The particle size and zeta potential: to evaluate the hydrodynamic diameter and surface charge stability of the N-CDs in solution, dynamic light scattering (DLS) analysis was performed. The particle size distribution and surface charge were measured with a Nano-ZS 90 instrument from Malvern at 25 °C.

•Fourier transform infrared (FT-IR) spectroscopy: FT-IR analysis was conducted to identify the surface functional groups and chemical bonds present in the N-CDs. Spectra of N-CDs powder were recorded at room temperature using a PerkinElmer Spectrum 1000 FT-IR spectrometer in the range of 400–4000 cm^{-1}.

•Thermogravimetric analysis (TGA): this test was performed to assess the thermal stability and decomposition behavior of the N-CDs. TGA was conducted using a TG 209 F1 Iris thermal-microbalance (Netzsch) in a nitrogen atmosphere, with a flow rate of 30 mL min^{-1} and a heating ramp of 3 °C min^{-1} up to 600 °C.

•UV-Vis absorption: to investigate the optical absorption features and electronic transitions of the N-CDs, UV-Vis absorption spectroscopy was employed. Measurement were made using a PerkinElmer Lambda 365 UV-Vis-NIR spectrometer.

•Emission and excitation spectra: these spectra were recorded to analyze the luminescent properties and excitation-dependent behavior of the N-CDs. Measurement were carried out at room temperature using a Fluoromax 4P model Horiba spectrometer with a xenon arc lamp as the excitation source.

•Photoluminescence quantum yield (PLQY): PLQY was determined to quantify the fluorescence efficiency of the N-CDs. Measurements were performed using a compact integrating sphere coupled with a Horiba spectrometer.

•Temperature-dependent emission: this test aimed to study the thermal sensitivity of the luminescence for potential applications in optical thermometry. Emission Measurements were conducted using a JOBIN YVON HR 320 spectrometer with temperature control.

3. Results and discussion

3.1. Structural characterization of N-CDs

As shown in Fig. 2a and b, the morphology of the carbon dots (CDs) was obtained through transmission electron microscopy (TEM) observations of a dilute drop of the prepared suspension, which revealed tiny spherical nanoparticles (NPs) with sizes in the range of [9–10 nm]. Additional information about the size of the N-CDs was provided by dynamic light scattering (DLS), which measures the size distribution based on the hydrodynamic volume of the particles (Fig. 2c). The DLS results show a monomodal distribution with a peak at approximately 10 nm. The ζ-potential of the QDs at pH 6 was around −15 mV, indicating that the CDs were negatively charged. Though the ζ-potential is moderate in absolute value, the presence of these negative charge contributed to prevent the aggregation of the CDs NPs, and ensure long term colloidal stability without any risk of aggregation.

The FTIR spectra of N-CDs is shown in Fig. 2d and was superimposed with that of CA to highlight the change in the band after the hydrothermal treatment. The spectrum of CDs is characterized by bands at 1750, 1695, 1650, 1550, 1400, 1340, 1300, 1160, and 1150 cm^{-1}. We assign the band at 1695, 1650 and 1550 cm^{-1} to amid groups (amid II and amide I) most likely resulting from the reaction between the carboxylic acid groups of CA and the amine groups of TREN.[50,51] This region

Open Access Article. Published on 30 May 2025. Downloaded on 11/9/2025 1:50:11 PM.
This article is licensed under a Creative Commons Attribution-NonCommercial 3.0 Unported Licence.

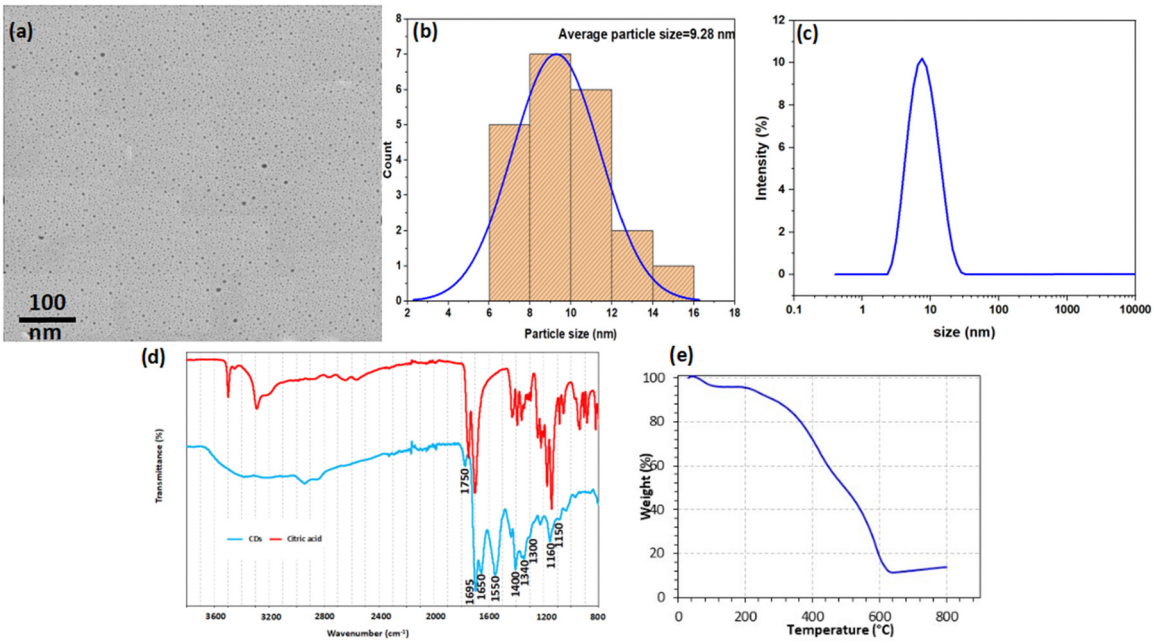

Fig. 2 (a) TEM image (b) the histogram of the size for the N-CDs, (c) the hydrodynamic size, (d) FTIR spectra of CA and N-CDs, and (e) thermogravimetric analysis curve of CDs.

encompasses also the stretching vibration of C═C polycyclic aromatic hydrocarbons. The presence of band at 1750 cm^{-1} suggested also the existence of carbonyl (C═O) groups.[52] The 1300–1000 cm^{-1} region included the contribution of different groups including C–O, C–N, C═C and phenol.[53–59]

The absence of symmetric and asymmetric peaks of CH_2 at 2920 and 2850 cm^{-1}, in the N-CDs FTIR spectra indicate that the carbon source was fully carbonized into graphitic structure.

The TGA of a lyophilised sample of N-CDs, shown in Fig. 2e, is characterized by a first weight loss of about 5% due to the evaporation of residual water in the lyophilized powder, followed by a steep degradation starting at 200 °C and continuing up to 600 °C. The loss from 200 to 350 °C, and involving the decomposition and oxidation of the carbon skeleton. The decomposition of the different functional groups (carbonyl, amide, amine, phenol and groups) from the surface of the N-CDs occurred in the range of 350–400 °C, while scission of the aromatic skeletal rings should occur over 500 °C.

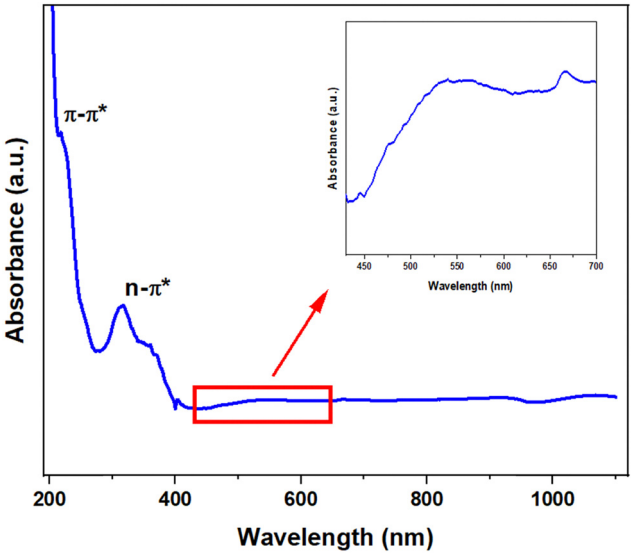

Fig. 3 UV Vis absorption spectrum of N-CDs.

3.2. Optical characterization of N-CDs

The optical properties of the N-CDs were investigated using UV-Vis absorption spectroscopy. Fig. 3 shows the UV-Vis spectrum of a diluted aqueous solution of the N-CDs. Two distinct absorption peaks are clearly observed in the spectrum. The peak at approximately 217 nm is attributed to π–π* transitions within the aromatic C═C bonds, which are indicative of the sp^2-π conjugation domain.[60,61] Furthermore, an absorption band ranging from 285 to 400 nm is associated with n–π* transitions, originating from surface functional groups that contain lone electron pairs.[62,63] These findings highlight the presence of both conjugated structures and surface-functionalized moieties in the N-CDs, contributing to their unique optical characteristics.

The fluorescence properties of the N-CDs were thoroughly investigated using photoluminescence (PL) spectroscopy. As shown in Fig. 4a, the excitation spectrum (red line) exhibits two peaks at 258 nm and 380 nm. Upon excitation at 380 nm, the fluorescence emission spectrum reveals a strong emission peak at 450 nm. The high fluorescence performance of the N-CDs is demonstrated in the inset of Fig. 4a, where the bright blue emission underscores their exceptional photoluminescent properties. This remarkable fluorescence intensity and stability

 © 2025 The Author(s). Published by the Royal Society of Chemistry

Open Access Article. Published on 30 May 2025. Downloaded on 11/9/2025 1:50:11 PM.
This article is licensed under a Creative Commons Attribution-NonCommercial 3.0 Unported Licence.

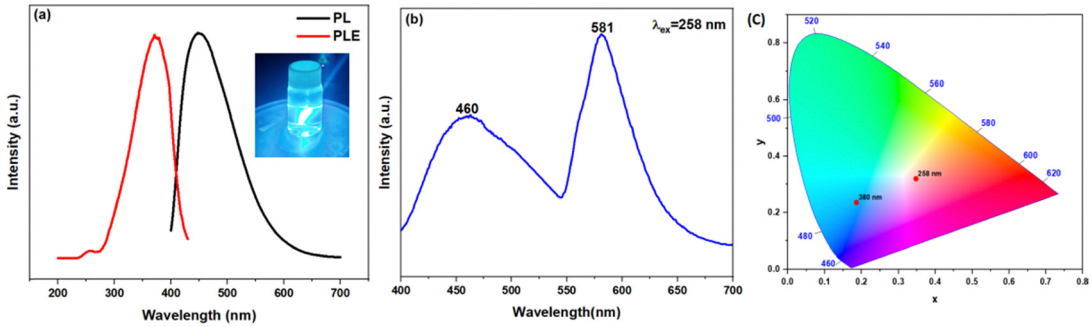

Fig. 4 (a) Excitation spectrum of the CDs recorded by monitoring the emission at 450 nm, and emission spectrum obtained under excitation at 380 nm. Inset shows blue fluorescence under 375 nm laser excitation, (b) emission spectrum of N-CDs under 258 nm excitation, and (c) chromaticity coordinates of N-CDs under 258 nm and 380 nm excitation.

make the N-CDs highly suitable for applications such as bioimaging, chemical sensing, and optoelectronic devices.

Furthermore, under an excitation wavelength of 258 nm (Fig. 4b), dual emission bands are observed, cantered at 460 nm and 581 nm, corresponding to blue and red emissions, respectively. The origins of these distinct emission bands can be rationalized based on the UV-Vis absorption spectrum. The blue emission at 460 nm is attributed to the absorption band between 285 and 400 nm, which is often associated with energy trapping by surface states.[64,65] On the other hand, the red emission at 581 nm corresponds to the visible-range absorption bands (as seen in the inset of Fig. 3), typically linked to transitions involving surface functional groups.[66–68]

To further explore the fluorescence characteristics of the N-CDs, excitation-dependent emission spectra were recorded by varying the excitation wavelengths from 350 nm to 390 nm in 5 nm increments (Fig. 5). The results indicate that the emission intensity gradually increases with higher excitation wavelengths. Notably, unlike many previously reported CDs,[69,70] the PL emission peaks of the synthesized N-CDs remain constant regardless of changes in the excitation wavelength. This unique behaviour is likely due to π–π* transitions within the graphitic carbon cores,[71] highlighting the robust optical properties of the CDs.

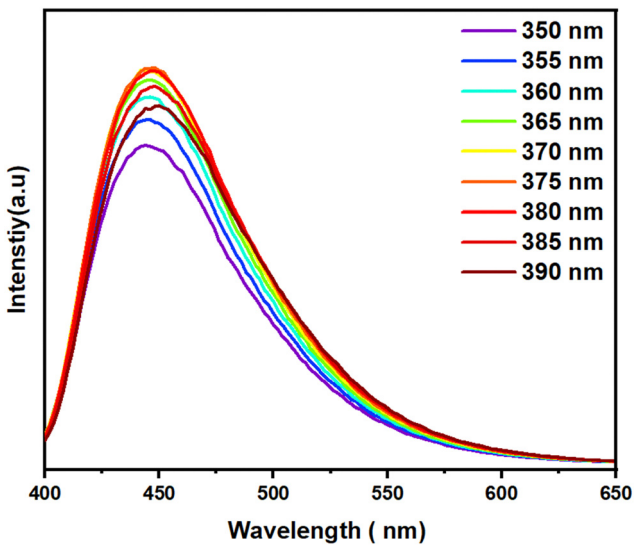

Fig. 5 Fluorescence emission spectra of N-CDs obtained at different excitation wavelengths progressively increasing from 350 to 390 nm in 5 nm increments.

The quantum yield (QY) of the CDs was determined using the integrating sphere method, which provides an absolute measurement by directly quantifying the emitted and absorbed photons. The general formula is as follows:[72]

$$\mathrm{QY} = \frac{\text{Number of photons emitted}}{\text{Number of photons absorbed}} \tag{1}$$

The synthesized N-CDs exhibited an exceptionally high QY of 90.85%, which can be attributed to the efficient energy transfer mechanisms enabled by their well-defined structural and surface properties. The use of citric acid as a carbon source, coupled with TREN as a nitrogen-rich passivating agent, likely contributed to the formation of surface states that enhance radiative recombination. Additionally, the hydrothermal process promoted uniform size distribution and minimized non-radiative pathways, further boosting the fluorescence efficiency.

3.3. Temperature-dependent fluorescence

To investigate the thermometric behaviour of the N-CDs, emission spectra were recorded under 380 nm excitation across a temperature range of 298 K to 343 K (Fig. 6a). The results clearly demonstrate a progressive decrease in luminescence intensity and integrated emission area by approximately 64% as the temperature increased, without any spectral shifts. This temperature-dependent luminescence behaviour can be attributed to thermal activation, which promotes increased non-radiative decay pathways.[73–75]

As illustrated in Fig. 6b, the fluorescence intensity ratio $\Delta = I/I_0$ (where I_0 is the maximum fluorescence intensity) decreases linearly with rising temperature, exhibiting a highly linear response with a coefficient of determination $R^2 = 0.998$. This linearity enabled the calculation of relative thermal sensitivity (S_r) using the following formula:[73]

$$S_r = \frac{1}{\Delta}\left|\frac{\partial \Delta}{\partial T}\right| \tag{2}$$

Open Access Article. Published on 30 May 2025. Downloaded on 11/9/2025 1:50:11 PM.
This article is licensed under a Creative Commons Attribution-NonCommercial 3.0 Unported Licence.

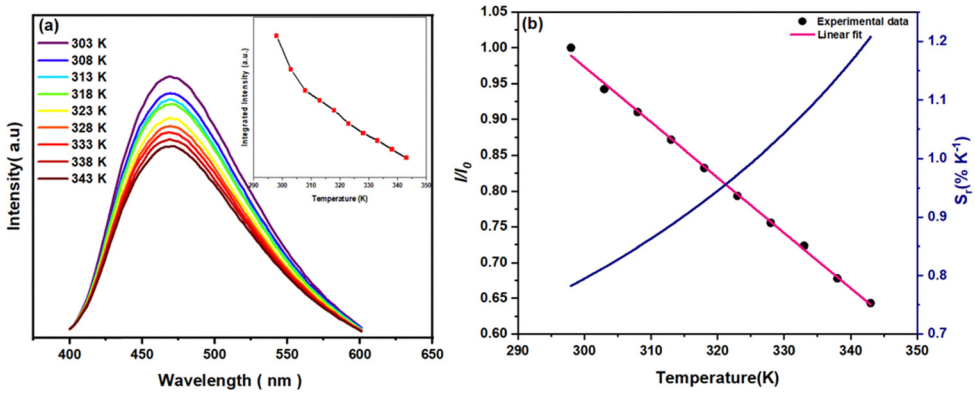

Fig. 6 (a) PL spectra of N-CDs as function of temperature under 380 nm excitation (Inset: Integrated intensity as function of temperature), (b) temperature dependence of the integrated intensity (linear dependence with R^2 = 0.998) and relative thermal sensitivity S_r.

A S_r value of approximately 1.21% K^{-1} was obtained at 343 K, indicating that the synthesized N-CDs hold significant promise for applications in *in vivo* temperature sensing.

3.4. Effect of pH on optical properties of N-CDs

The luminescence behaviour of N-CDs was further investigated across a pH range from 4 to 12. Fig. 7a shows the fluorescence spectra of N-CDs measured at an excitation wavelength of 380 nm. In order to estimate the pH sensitivity, the integrated intensity, the peak position and full widths at half-maximum (FWHM) of the fluorescence band are plotted as a function of pH, as shown in Fig. 7b–d, respectively. The PL intensity increases gradually with increase in pH, in contrast to the FWHM widths, which decreased by 22% at pH = 12. Moreover, a shift of the emission peak as a function of pH was observed from 464 nm for pH 4 to 447 nm for pH 12. The peak position of the emission bands change significantly with pH of the solution is likely due to the presence of functional groups liable to protonation like amide, amine, carboxylic function decorating the surface of the CDs.[76] The presence of these functional groups was supported by FTIR analysis.

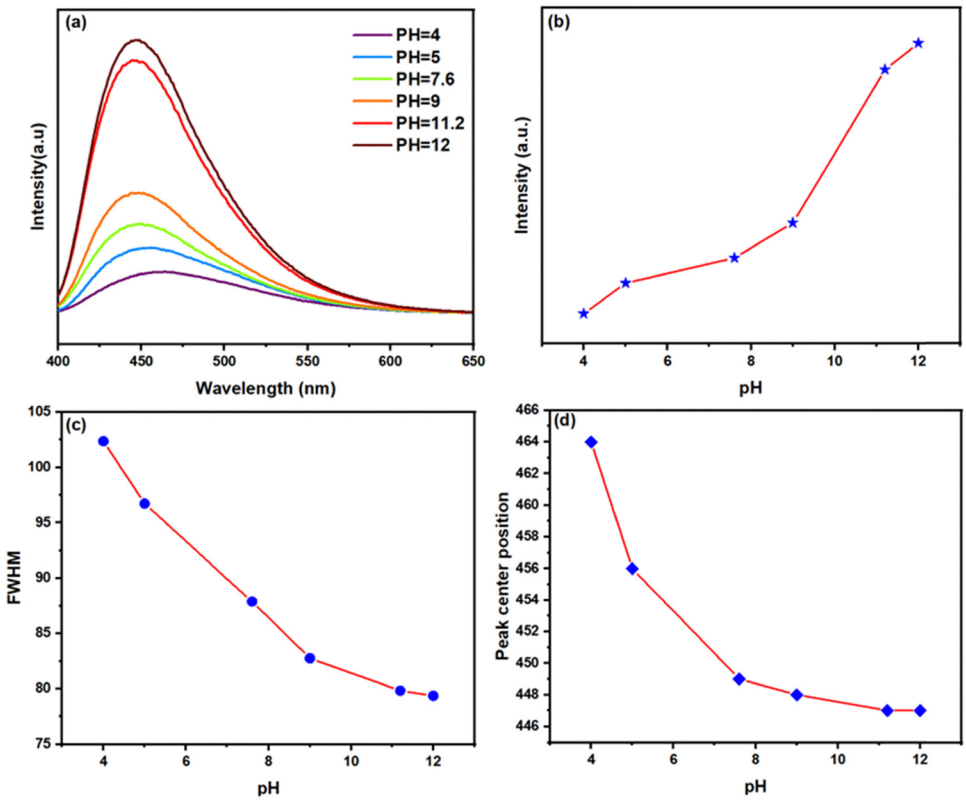

Fig. 7 (a) PL emission spectra, (b) PL intensity, (c) FWHM, and (d) peak center position of N-CDs in aqueous solution at pH values ranging from 4 to 12, under 380 nm excitation wavelength.

 © 2025 The Author(s). Published by the Royal Society of Chemistry

Open Access Article. Published on 30 May 2025. Downloaded on 11/9/2025 1:50:11 PM.
This article is licensed under a Creative Commons Attribution-NonCommercial 3.0 Unported Licence.

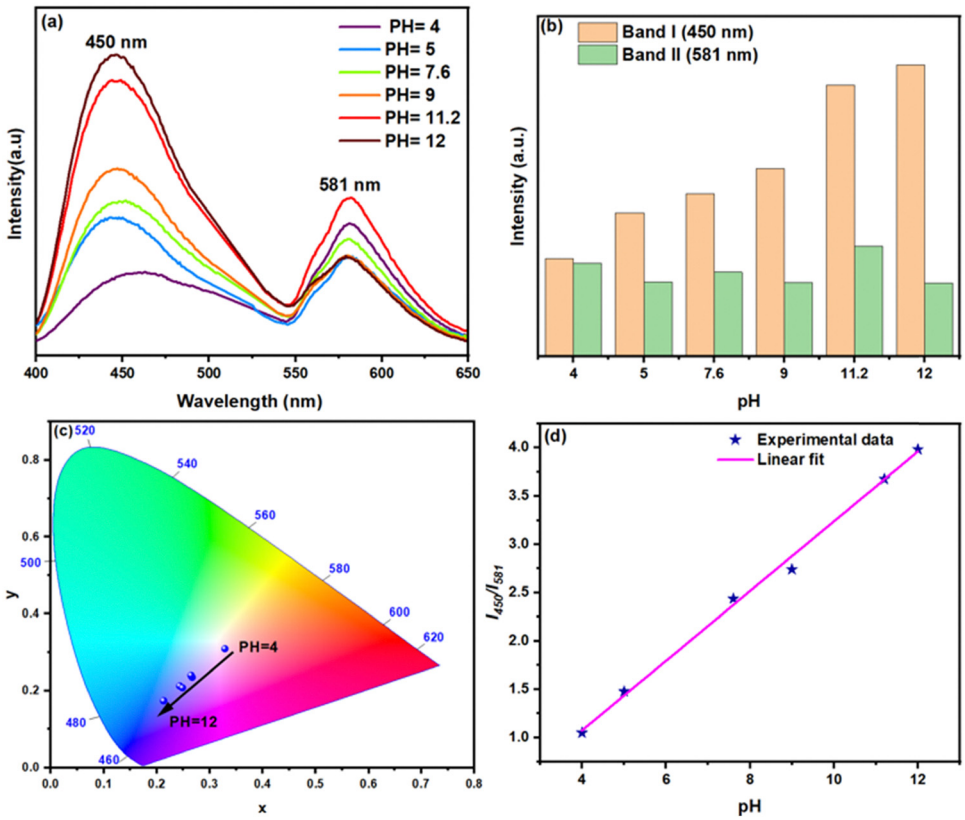

Fig. 8 (a) The emission spectra of N-CDs as a function of pH under 258 nm excitation, (b) the variation of fluorescence intensity of Band I and band II, (c) the Chromaticity diagram, and (d) the corresponding intensity ratio as a function of pH and the fitted curve.

Under 258 nm excitation, the fluorescence spectra shown in Fig. 8a reveal a dominant emission band cantered at 581 nm (red band) at low pH (pH = 4), while the band cantered at 450 nm (blue band) appeared weaker. The 446 nm emission band is primarily associated with surface amino-related impurity levels, which are influenced by the acidity of the solution.[77] As the pH increased, the intensity of the blue band progressively rose, eventually becoming the dominant feature (Fig. 8b).

The chromaticity diagram (Fig. 8c) indicates a significant blue shift in fluorescence emission at pH 12. According to Kumari *et al.*,[78] this shift is attributed to changes in the surface state of the N-CDs. The presence of COO^- groups on the surface modifies the electronic structure by removing certain energy levels, reducing the number of electronic transitions, and causing a blue shift in photoluminescence (PL) emission.

Furthermore, Fig. 8d plots the intensity ratio of the blue band to the red band as a function of pH, showing a linear increase with rising pH. These results confirm that the PL intensities of the blue and red bands are highly sensitive to pH changes, making the N-CDs suitable candidates for use in ratiometric fluorescence-based pH sensing applications.

3.5. Selective fluorescence amplification of N-CDs aqueous solution in the presence of Hg^{2+}

Mercury ion (Hg^{2+}) is a highly toxic heavy metal and a persistent pollutant that poses a significant threat to human health due to its non-biodegradable nature. Previous studies have reported that carboxylic groups can bind to metal ions through metal–ligand interactions.[79] Consequently, the synthesized N-CDs solution serves as a promising sensor for Hg^{2+} detection in aqueous environments. All experiments were performed using the as-prepared N-CDs solution with a natural pH of ~4. This mildly acidic condition enhances the fluorescence response by favoring protonation of surface functional groups (*e.g.*, amino and carboxyl), which promotes effective coordination with Hg^{2+} ions.

Fig. 9a displays the emission spectra of N-CDs at various Hg^{2+} ion concentrations. The fluorescence intensity progressively increased with higher concentrations of Hg^{2+} under 380 nm excitation, without any shift in the emission peak position or change in spectral shape. As shown in Fig. 9b, the fluorescence intensity ratio I/I_0 (where I_0 and I represent the fluorescence intensities in the absence and presence of Hg^{2+}, respectively) demonstrated a linear increase with Hg^{2+} concentration, exhibiting excellent linearity with a correlation coefficient of 0.994 over the range of 0–10 μM (Fig. 9c).

The limit of detection (LOD) for Hg^{2+} was calculated using the equation:

$$\mathrm{LOD} = \frac{3\sigma}{S} \tag{3}$$

Open Access Article. Published on 30 May 2025. Downloaded on 11/9/2025 1:50:11 PM.
This article is licensed under a Creative Commons Attribution-NonCommercial 3.0 Unported Licence.

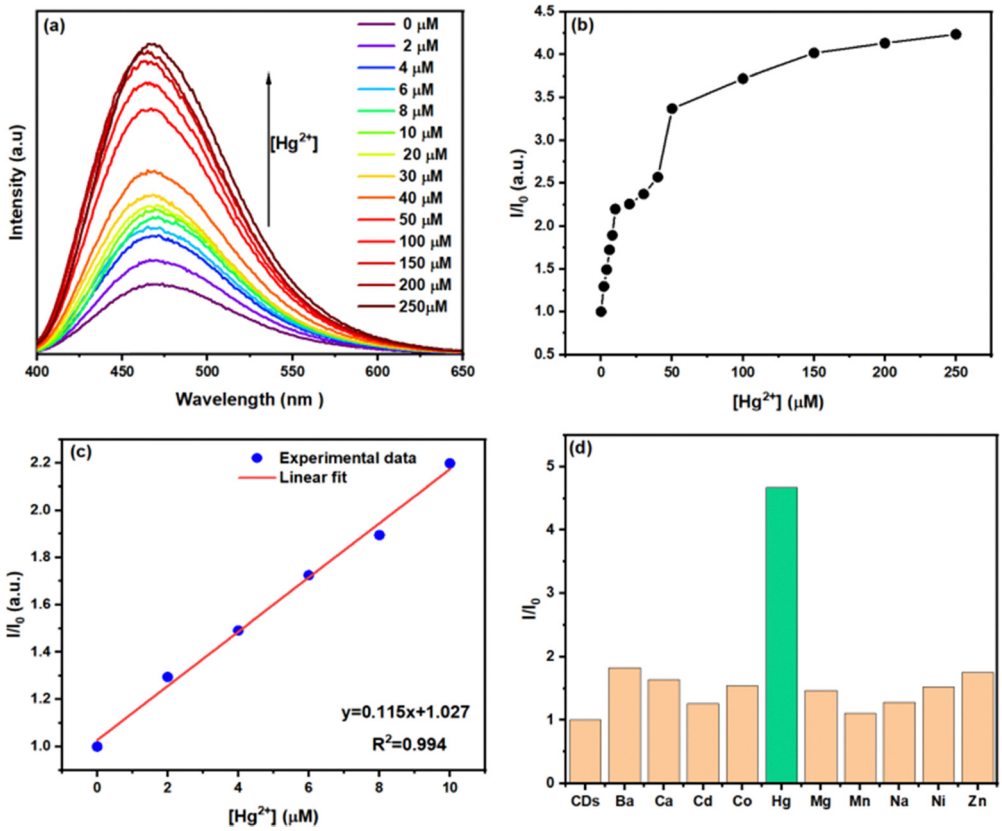

Fig. 9 (a) Fluorescent emission spectra of N-CDs in the presence of difference Hg^{2+} concentrations, (b) The dependence of I/I_0 on the concentrations of Hg^{2+} within the range of 0–250 μM, (c) the dependence of I/I_0 on the concentrations of Hg^{2+} within the range of 0–10 μM, and (d) relative fluorescence intensities of N-CDs in the presence of different metal ions under 380 nm excitation (the concentration of metal ions is 250 μM).

Table 1 Sensitivity of various nano sensors for detection of Hg^{2+}

Materials	Sources of CDs	Linear range (μM)	LOD (μM)	Ref.
CQDs	Citric acid	20–200	5.7	81
CDs	Eggshell membrane	10–100	2.6	82
CDs-LAPONITE®	—	1–40	2.5	83
Eu/CDs	EDTA, L-cysteinec, and ethylene glycol	5–250	2.2	84
N,S/C-dots	Citric acid, urea and L-cysteine	0–40	2	85
N,S-CDs	Citric acid and L-glutathione	5–50	1.78	86
N,S-CDs	Glycerol and cysteine	1–75	0.5	47
AuNPs/CDs	Glutathione and ethyl alcohol	0.5–15	0.5	87
N-CDs	Citric acid and tri-(2-aminoethyl)amine	0–10	0.46	This work
N-CDs	Citric acid and melamine	2–14	0.44	46
N/S-CDs	Gardenia fruits	2–20	0.32	88
S-CDs	citric acid and sodium sulfite	0.5–180	0.2	89

where σ is the standard deviation of the I/I_0 values and s is the slope of the linear plot.[80]

The calculated LOD was approximately 0.46 μM. Table 1 compares the detection limits of various fluorescence-based sensors for Hg^{2+}, demonstrating that the synthesized N-CDs exhibit superior performance, with a notably lower LOD than many previously reported materials. However, although this LOD represents an improvement over existing methods, it remains higher than the maximum permissible levels for Hg^{2+} in drinking water, as set by the European Union (5 nM) and the US Environmental Protection Agency (10 nM).[90] Therefore, further optimization of the sensing platform is necessary to enable ultra-trace detection suitable for regulatory environmental monitoring.

Table 2 Determination of Hg^{2+} in real water samples using N-CDs and recovery calculation

Sample Type	Added Hg^{2+} (μM)	Detected Hg^{2+} (μM)	Recovery (%)	RSD (%) (n = 3)
Tap water	2.00	1.96	98.0	2.1
Tap water	5.00	5.18	103.6	1.8
Tap water	8.00	7.62	95.3	2.5

 © 2025 The Author(s). Published by the Royal Society of Chemistry

Open Access Article. Published on 30 May 2025. Downloaded on 11/9/2025 1:50:11 PM.
This article is licensed under a Creative Commons Attribution-NonCommercial 3.0 Unported Licence.

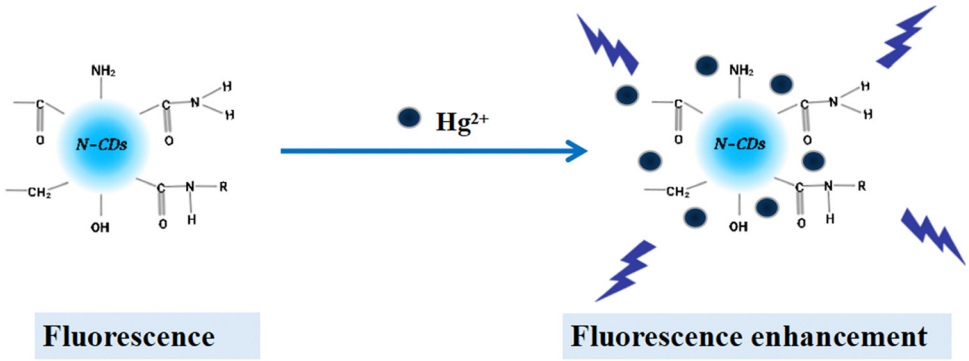

Fig. 10 The schematic mechanism of fluorescence emission enhancement of the N-CDs by Hg^{2+}.

To assess the selectivity of the N-CDs for Hg^{2+}, the fluorescence enhancement efficiency in the presence of various metal ions, including Co^{2+}, Mg^{2+}, Ba^{2+}, Ca^{2+}, Zn^{2+}, Cd^{2+}, Mn^{2+}, Ni^{2+}, and Na^{+}, was measured. Fig. 9d illustrates the relative fluorescence intensity ratio I/I_0 for each metal ion. The results clearly indicate that the N-CDs exhibited a specific and strong response to Hg^{2+} ions compared to other metal ions. This exceptional selectivity confirms the potential of the CDs for sensitive and selective Hg^{2+} detection in aqueous solutions.

To evaluate the practical applicability of the developed N-CDs-based fluorescence sensor, we applied the method to the detection of Hg^{2+} ions in real water samples. Tap water was collected, filtered to remove particulates, and subsequently spiked with known concentrations of Hg^{2+} (2 μM, 4 μM, 6 μM, 8 μM and 10 μM). The samples were then analysed under the same experimental conditions described previously, and the detected Hg^{2+} concentrations were determined using the calibration curve based on the fluorescence intensity ratio (I/I_0). The recoveries were calculated using the formula:[91]

$$\text{Recovery } (\%) = \frac{\text{Detected concentration}}{\text{Added concentration}} \times 100 \qquad (4)$$

As shown in Table 2, the recoveries ranged from 95.3% to 100.5%. Recovery values close to 100% indicate good accuracy. These results demonstrate that the proposed fluorescence sensor is effective and reliable for the detection of Hg^{2+} in complex real-water matrices.

3.6. Sensing mechanism of N-CDs toward Hg^{2+} ions

The fluorescence enhancement observed upon addition of Hg^{2+} ions to the N-CDs solution is attributed to a "turn-on" mechanism. This behavior is likely due to specific coordination between Hg^{2+} ions and the electron-rich functional groups (*e.g.*, amino, hydroxyl, and carboxyl) present on the surface of the N-CDs. The coordination with Hg^{2+} may passivate surface defect states that otherwise act as non-radiative recombination centers, thereby improving the radiative recombination efficiency and enhancing the fluorescence intensity. In addition, this interaction may rigidify the surface structure or alter the electronic environment of the fluorophores, further promoting fluorescence emission. A schematic illustration of the proposed sensing mechanism is presented in Fig. 10.

4. Conclusion

In this study, highly photoluminescent nitrogen-doped carbon dots (N-CDs) were synthesized *via* a hydrothermal method using citric acid and tri(2-aminoethyl)amine. The N-CDs exhibited an exceptional quantum yield of 90%, among the highest reported for undoped carbon dots, along with dual fluorescence emission at 450 nm (under 380 nm excitation) and 460/581 nm (under 258 nm excitation). These optical properties enabled multifunctional applications, including temperature-dependent fluorescence with a linear sensitivity of 1.21% K^{-1} over the range of 298–343 K. The N-CDs also demonstrated pH-responsive behavior, with the fluorescence intensity ratio (I_{450}/I_{581}) showing a linear response across the pH range of 4–12. Furthermore, the N-CDs enabled selective detection of Hg^{2+} ions through fluorescence enhancement, displaying a linear response over the range of 0–10 μM and a detection limit of 0.46 μM outperforming many surface-modified carbon dot systems. The synergy of high quantum efficiency, dual-emission versatility, and quantitative sensitivity across temperature, pH, and Hg^{2+} detection underscores the potential of these N-CDs as a versatile platform for environmental monitoring and biomedical diagnostics. Notably, their detection limit for Hg^{2+} complies with stringent regulatory standards for water quality. This work advances the development of multifunctional nanomaterials, offering a promising blueprint for unmodified carbon dots with real-world applicability in sensing technologies.

Data availability

All data underlying the results are available as part of the article and no additional source data are required.

Conflicts of interest

There are conflcts to declare.

References

1 N. K. Tan, H. Chan, Z. Lu, H. Zreiqat, G. Lakhwani, P. Lesani and E. J. New, Advancements in Bioactive Nanomaterials for

Open Access Article. Published on 30 May 2025. Downloaded on 11/9/2025 1:50:11 PM.
This article is licensed under a Creative Commons Attribution-NonCommercial 3.0 Unported Licence.

Tissue Engineering Applications, *ACS Appl. Mater. Interfaces*, 2024, **16**, 47303–47313.
2 Y. Hailing, L. Xiufang, W. Lili, L. Baoqiang, H. Kaichen, H. Yongquan, Z. Qianqian, M. Chaoming, R. Xiaoshuai, Z. Rui, L. Hui, P. Pengfei and S. Hong, Nanoparticle-Based Drug Delivery Systems for Cancer Therapy, *Nanoscale*, 2020, **12**, 17222.
3 L. Vallan and H. Imahori, Recent Advances in Organic Photovoltaics: From Molecular Design to Device Performance, *ACS Appl. Electron. Mater.*, 2022, **4**, 4231–4257.
4 M. Alafeef, I. Srivastava, T. Aditya and D. Pan, Carbon Quantum Dots for Biomedical Imaging and Sensing, *Small*, 2024, **20**, 2303937.
5 P. Zhu, Z. Cheng, L. Du, Q. Chen and K. Tan, Surface Chemistry of Graphene Oxide and Its Applications in Environmental Remediation, *Langmuir*, 2018, **34**, 9982–9989.
6 A. Truskewycz, H. Yin, N. Halberg, D. T. H. Lai, A. S. Ball, V. K. Truong, A. M. Rybicka and I. Cole, Antimicrobial Nanocoatings for Medical Devices: A Review, *Small*, 2022, **18**, 2106342.
7 T. Feng, X. Ai, G. An, P. Yang and Y. Zhao, Luminescent Metal Nanoclusters for Bioimaging and Theranostics, *ACS Nano*, 2016, **10**, 4410.
8 L. Cao, M. Meziani, S. Sahu and Y. Sun, Carbon Dots: Synthesis, Properties, and Applications, *Acc. Chem. Res.*, 2013, **46**, 171.
9 W. Li, Z. Zhang, B. Kong, S. Feng, J. Wang, L. Wang, J. Yang, F. Zhang, P. Wu and D. Zhao, Mesoporous Silica Nanoparticles for Controlled Drug Delivery, *Angew. Chem., Int. Ed.*, 2013, **52**, 8151.
10 K. Qu, J. Wang, J. Ren and X. Qu, Functionalized Graphene Oxide for Targeted Drug Delivery, *Chem. – Eur. J.*, 2013, **19**, 7243.
11 Y. Chen, M. Zheng, Y. Xiao, H. Dong, H. Zhang, H. Hu, B. Lei and Y. Liu, Graphene Quantum Dots for Optoelectronic Applications, *Adv. Mater.*, 2016, **28**, 312.
12 S. K. Panda, S. G. Hickey, H. V. Demir and A. Eychmüller, Colloidal Semiconductor Nanocrystals for Light-Emitting Diodes, *Angew. Chem., Int. Ed.*, 2011, **50**, 4432.
13 Z. Sheffield, M. Alafeef, P. Moitra, P. Ray and D. Pan, Carbon Dots for Environmental Monitoring and Remediation, *Nanoscale*, 2022, **14**, 5112.
14 M. Alafeef, K. Dighe, P. Moitra and D. Pan, Sustainable Synthesis of Carbon Dots for Biosensing Applications, *ACS Sustainable Chem. Eng.*, 2022, **10**, 245.
15 P. Ray, P. Moitra and D. Pan, Carbon Dots as Versatile Nanomaterials for Energy Conversion and Storage, *View*, 2022, **3**, 26.
16 D. Sar, F. Ostadhossein, P. Moitra, M. Alafeef and D. Pan, Carbon Dot-Based Nanocomposites for Enhanced Photocatalytic Activity, *Adv. Sci.*, 2022, **9**, 2202414.
17 Y. Sun, B. Zhou, Y. Lin, W. Wang, K. A. S. Fernando, P. Pathak, M. J. Meziani, B. A. Harruff, X. Wang, H. Wang, P. G. Luo, H. Yang, M. E. Kose, B. Chen, L. M. Veca and S. Xie, Quantum-Sized Carbon Dots for Bright and Colorful Photoluminescence, *J. Am. Chem. Soc.*, 2006, **128**, 7756–7757.
18 H. Peng and J. Travas-Sejdic, Simple Aqueous Solution Route to Luminescent Carbon Dots from Carbohydrates, *Chem. Mater.*, 2009, **21**, 5563–5565.
19 Z. Ma, H. Ming, H. Huang, Y. Liu and Z. Kang, One-Step Hydrothermal Synthesis of Highly Luminescent Carbon Dots, *New J. Chem.*, 2012, **36**, 861.
20 R. Zhang and W. Chen, Carbon Dots for Electrochemical Sensing of Biomolecules, *Biosens. Bioelectron.*, 2014, **55**, 83–90.
21 Y. Guo, Z. Wang, H. Shao and X. Jiang, Synthesis of Fluorescent Carbon Dots with Tunable Emission Using Citric Acid and Urea, *Carbon*, 2013, **52**, 583–589.
22 R. Fan, Q. Sun, L. Zhang, Y. Zhang and A. Lu, Green Synthesis of Carbon Dots from Glucose and Their Application as a Fluorescent Probe, *Carbon*, 2014, **71**, 87–93.
23 Y. Zhang, D. Ma, Y. Zhuang, X. Zhang, W. Chen, L. Hong, Q. Yan, K. Yu and S. Huang, Fluorescent Carbon Dots Derived from Citric Acid and Ethylenediamine for Cell Imaging, *J. Mater. Chem.*, 2012, **22**, 16714.
24 Y. Liu, N. Xiao, N. Gong, H. Wang, X. Shi, W. Gu and L. Ye, A Facile One-Step Hydrothermal Synthesis of Photoluminescent Carbon Dots, *Carbon*, 2014, **68**, 258–264.
25 X. Gao, Y. Lu, R. Zhang, S. He, J. Ju, M. Liu, L. Lia and W. Chen, One-Pot Hydrothermal Synthesis of Nitrogen-Doped Carbon Dots for Cell Imaging, *J. Mater. Chem. C*, 2015, **3**, 2302–2309.
26 W. Lu, Y. Jiao, Y. Gao, J. Qiao, M. Mozneb, S. Shuang, C. Dong and C. Li, Nitrogen-Doped Carbon Dots for Fluorescent Detection of Fe^{3+} Ions, *ACS Appl. Mater. Interfaces*, 2018, **10**, 42915–42924.
27 P. Das, M. Maruthapandi, A. Saravanan, M. Natan, G. Jacobi, E. Banin and A. Gedanken, Carbon Dots for Heavy-Metal Sensing, pH-Sensitive Cargo Delivery, and Antibacterial Applications, *ACS Appl. Nano Mater.*, 2020, **3**, 11777–11790.
28 G. Dong, K. Lang, H. Ouyang, W. Zhang, L. Bai, S. Chen, Z. Zhang, Y. Gao, Z. Mu and X. Zhao, Carbon Dots Prepared by Hydrothermal Treatment of Dopamine as an Effective Fluorescent Sensing Platform for the Label-Free Detection of Iron(III) Ions, *RSC Adv.*, 2020, **10**, 33483.
29 C. Wang, H. Lin, Z. Xu, Y. Huang, M. G. Humphrey and C. Zhang, Tunable Carbon-Dot-Based Dual-Emission Fluorescent Nanohybrids for Ratiometric Optical Thermometry in Living Cells, *ACS Appl. Mater. Interfaces*, 2016, **8**(10), 6621–6628.
30 C. Wang, Z. Xu, H. Cheng, H. Lin, M. G. Humphrey and C. Zhang, A hydrothermal route to water-stable luminescent carbon dots as nanosensors for pH and temperature, *Carbon*, 2015, **82**, 87–95.
31 P. Yu, X. Wen, Y. Toh and J. Tang, Synthesis of Highly Fluorescent Carbon Dots via Microwave Heating, *J. Phys. Chem. C*, 2012, **116**, 25552–25557.
32 Z. L. Wu, M. X. Gao, T. T. Wang, X. Y. Wan, L. L. Zheng and C. Z. Huang, Facile Synthesis of Nitrogen-Doped Carbon Dots for Multicolor Imaging, *Nanoscale*, 2014, **6**, 3868–3874.
33 F. Ahmed, S. Iqbal, L. Zhao and H. Xiong, Highly Fluorescent Carbon Dots for Selective Detection of Cr(VI), *Anal. Chim. Acta*, 2021, **1183**, 338977.

 © 2025 The Author(s). Published by the Royal Society of Chemistry

Open Access Article. Published on 30 May 2025. Downloaded on 11/9/2025 1:50:11 PM.
This article is licensed under a Creative Commons Attribution-NonCommercial 3.0 Unported Licence.

34 C. Wang, Z. Xu, H. Cheng, H. Lin, M. G. Humphrey and C. Zhang, Photoluminescent Carbon Dots from Citric Acid and Urea: Formation Mechanism and Application in Cell Imaging, *Carbon*, 2015, **82**, 87–95.
35 X. Jia, J. Lia and E. Wang, One-Pot Hydrothermal Synthesis of Highly Luminescent Nitrogen-Doped Carbon Dots, *Nanoscale*, 2012, **4**, 5572–5575.
36 P. Das, S. Ganguly, P. Khoshbakht Marvi, M. Sherazee, X. Tang, S. Srinivasan and A. R. Rajabzadeh, Carbon Dots Infused 3D Printed Cephalopod Mimetic Bactericidal and Antioxidant Hydrogel for Uniaxial Mechano-Fluorescent Tactile Sensor, *Adv. Mater.*, 2024, **36**, 2409819.
37 R. Long, C. Tang, T. Li, X. Tong, C. Tong, Y. Guo, Q. Gao, L. Wu and S. Shi, Dual-emissive carbon dots for dual-channel ratiometric fluorometric determination of pH and mercury ion and intracellular imaging, *Microchim. Acta*, 2020, **187**, 307.
38 C. Xia, M. Cao, J. Xia, G. Zhou, D. Jiang, D. Zhang, J. Wang and H. Li, Nitrogen-Doped Carbon Dots for Fluorescent Detection of Cu^{2+} Ions, *J. Mater. Chem. C*, 2019, **7**, 2563–2569.
39 W. Song, W. Duan, Y. Liu, Z. Ye, Y. Chen, H. Chen, S. Qi, J. Wu, D. Liu and L. Xiao, Fluorescent Carbon Dots for Sensitive Detection of Mercury Ions, *Anal. Chem.*, 2017, **89**, 13626–13633.
40 J. Shangguan, D. He, X. He, K. Wang, F. Xu, J. Liu, J. Tang, X. Yang and J. Huang, Carbon Dots for Fluorescent Detection of Cr(VI) in Water Samples, *Anal. Chem.*, 2016, **88**, 7837–7843.
41 C. Zhou, S. Wu, S. Qi, W. Song and C. Sun, Development of Carbon Dots for Heavy Metal Ion Detection, *J. Anal. Methods Chem.*, 2021, 6695354.
42 J. Pei, H. Li, F. Chen, Z. Chen, X. Yuan, Z. Han, D. Chen, D. Yu and D. Zhang, Functionalized Carbon Dots for Sensitive Detection of Fe^{3+} Ions, *ACS Appl. Mater. Interfaces*, 2024, **16**, 60819–60827.
43 S. Mandal, J. Pal, R. Subramanian and P. Das, Highly Luminescent Carbon Dots for White Light Emission, *Nano Res.*, 2020, **13**, 2770–2776.
44 Z. Wang, X. Yu, F. Li, F. Kong, W. Lv, D. Fan and W. Wang, Carbon Dots for Fluorescent Detection of Cu^{2+} Ions in Water, *Microchim. Acta*, 2017, **184**, 4775–4783.
45 K. Jiang, S. Sun, L. Zhang, Y. Wang, C. Cai and H. Lin, Red-Emitting Carbon Dots for Two-Photon Fluorescence Bio-imaging, *ACS Appl. Mater. Interfaces*, 2015, **7**, 23231–23238.
46 M. Szmyt, B. Buszewski and R. Kopciuch, Characterization of Carbon Dots by FTIR Spectroscopy, *Spectrochim. Acta, Part A*, 2020, **236**, 118320.
47 Y. Xu, H. Li, B. Wang, H. Liu, L. Zhao, T. Zhou, M. Liu, N. Huang, Y. Li, L. Ding and Y. Chen, One-Step Hydrothermal Synthesis of Carbon Dots for Fluorescent Detection of Fe^{3+} Ions, *Microchim. Acta*, 2018, **185**, 156.
48 K. Zhang, Y. Sang, Y. Gao, Q. Sun and W. Li, Synthesis of Nitrogen-Doped Carbon Dots for Detection of Fe^{3+} Ions, *Spectrochim. Acta, Part A*, 2022, **264**, 120281.
49 Q. Meng, F. Zhang, L. Wang, S. Xiang, S. Zhu, G. Zhang, K. Zhang and B. Yang, Carbon Dots for Fluorescent Detection of Cr(VI), *RSC Adv.*, 2014, **4**, 713–716.
50 D. Qu and Z. Sun, The formation mechanism and fluorophores of carbon dots synthesized via a bottom-up route, *Mater. Chem. Front.*, 2020, **4**, 400–420.
51 Z. Zhang, J. Hao, J. Zhang, B. Zhang and J. Tang, Protein as the source for synthesizing fluorescent carbon dots by a one-pot hydrothermal route, *RSC Adv.*, 2012, **2**, 8599–8601.
52 Y. Di, W. Liu, S. Shi, T. Wu, M. Wang and X. Liu, One-step synthesis of color-tunable carbon dots-based organic long persistent luminescence materials, *Chem. Eng. J.*, 2024, **479**, 147589.
53 H. Huang, H. Ge, Z. Ren, Z. Huang, M. Xu and X. Wang, Biocompatible Carbon Dots for Cellular Imaging and Drug Delivery, *Front. Bioeng. Biotechnol.*, 2021, **9**, 617097.
54 S. Chandra, A. R. Chowdhuri, T. K. Mahto, D. Laha and S. K. Sahu, Green Synthesis of Carbon Dots for Biological Applications, *Nano-Struct. Nano-Objects*, 2017, **12**, 10–18.
55 Q. H. Ye, F. Y. Yan, Y. M. Luo, Y. Y. Wang, X. G. Zhou and L. Chen, Fluorescent Carbon Dots for Selective Detection of Fe^{3+} Ions, *Spectrochim. Acta, Part A*, 2017, **173**, 854–862.
56 M. Y. Xue, Z. H. Zhan, M. B. Zou, L. L. Zhang and S. L. Zhao, One-Step Hydrothermal Synthesis of Carbon Dots for Detection of Fe^{3+} Ions, *New J. Chem.*, 2016, **40**, 1698–1703.
57 C. P. Han, R. Wang, K. Y. Wang, H. T. Xu, M. R. Sui, J. J. Li and K. Xu, Carbon Dots for Fluorescent Detection of Cu^{2+} Ions, *Biosens. Bioelectron.*, 2016, **83**, 229–236.
58 M. N. Egorova, A. N. Kapitonov, A. A. Alekseev and E. A. Obraztsova, Carbon Dots for Photodynamic Therapy, *J. Struct. Chem.*, 2020, **61**, 811–817.
59 W. J. Niu, Y. Li, R. Zhu, D. Shan, Y. Fan and X. Zhang, Carbon Dots for Electrochemical Detection of Heavy Metals, *Sens. Actuators, B*, 2015, **218**, 229–236.
60 B. Y. Han, X. S. Lei, D. Li, Q. D. Liu, Y. J. Chen, J. Wang and G. H. He, Carbon Dots for Photocatalytic Degradation of Organic Pollutants, *Adv. Opt. Mater.*, 2023, **11**, 2202293.
61 Z. Yu, F. Li and Q. Xiang, Carbon Dots for Solar Energy Conversion, *J. Mater. Sci. Technol.*, 2024, **175**, 244–257.
62 K. Jiang, S. Sun, L. Zhang, Y. Lu, A. Wu, C. Cai and H. Lin, Red-Emitting Carbon Dots for Two-Photon Fluorescence Imaging, *Angew. Chem., Int. Ed.*, 2015, **54**, 5360–5363.
63 W. Kwon, G. Lee, S. Do, T. Joo and S. W. Rhee, Size-Dependent Photoluminescence of Carbon Dots, *Small*, 2014, **10**, 506–513.
64 Y. Dong, H. Pang, H. B. Yang, C. Guo, J. Shao, Y. Chi, C. M. Li and T. Yu, Carbon-Based Dots Co-doped with Nitrogen and Sulfur for High Quantum Yield Fluorescence, *Angew. Chem., Int. Ed.*, 2013, **52**, 7800–7804.
65 P. Anilkumar, X. Wang, L. Cao, S. Sahu, J. H. Liu, P. Wang, K. Korch, K. N. Tackett, A. Parenzan and Y. P. Sun, Tunable Luminescent Carbon Nanodots, *Nanoscale*, 2011, **3**, 2023–2027.
66 T. Zhang, J. Zhu, Y. Zhai, H. Wang, X. Bai, B. Dong, H. Wang and H. Song, Carbon Dots for Fluorescent Detection of Heavy Metals, *Nanoscale*, 2017, **9**, 13042–13051.
67 H. Ding, S. B. Yu, J. S. Wei and H. M. Xiong, Full-Color Emission Carbon Dots, *ACS Nano*, 2016, **10**, 484–491.
68 D. Gao, X. Liu, D. Jiang, H. Zhao, Y. Zhu, X. Chen, H. Luo, H. Fan and X. Zhang, Nitrogen-Doped Carbon Dots for

Open Access Article. Published on 30 May 2025. Downloaded on 11/9/2025 1:50:11 PM.
This article is licensed under a Creative Commons Attribution-NonCommercial 3.0 Unported Licence.

Fluorescent Detection of Cu^{2+} Ions, *Sens. Actuators, B*, 2018, **277**, 373–380.

69 H. Sadhanala, S. Pagidi, S. Yadav, M. Beiderman, I. Grinberg, D. Fixler and A. Gedanken, Carbon Dots for Detection of Toxic Ions in Water, *ChemistrySelect*, 2022, **7**, e202201261.

70 C. Ma, Z. Zhu, H. Wang, X. Huang, X. Zhang, X. Qi, H. Zhang, Y. Zhu, X. Deng, Y. Peng, Y. Han and H. Zhang, Nitrogen-Doped Carbon Dots for Fluorescent Detection of Fe^{3+} Ions, *Nanoscale*, 2015, **7**, 10162–10169.

71 V. Arul and M. G. Sethuraman, Fluorescent Carbon Dots for Detection of Heavy Metal Ions, *Opt. Mater.*, 2018, **78**, 181–190.

72 Z. Yi, X. Li, H. Zhang, X. Ji, W. Sun, Y. Yu, Y. Liu, J. Huang, Z. Sarshar and M. Sain, Carbon Dots for Detection of Heavy Metals in Water, *Talanta*, 2021, **222**, 121663.

73 R. Wang, K. Q. Lu, Z. R. Tang and Y. J. Xu, Recent Progress in Carbon Dots: Synthesis, Properties and Applications in Photocatalysis, *J. Mater. Chem. A*, 2017, **5**, 3717–3734.

74 A. Sharma and J. Das, Small Molecules Derived Carbon Dots: Synthesis and Applications in Sensing, Catalysis, Imaging, and Biomedicine, *J. Nanobiotechnol.*, 2019, **17**, 92.

75 X. T. Zheng, A. Ananthanarayanan, K. Q. Luo and P. Chen, Glowing Graphene Quantum Dots and Carbon Dots: Properties, Syntheses, and Biological Applications, *Small*, 2015, **11**, 1620–1636.

76 J. Zhang, W. Shen, D. Pan, Z. Zhang, Y. Fang and M. Wu, Controlled Synthesis of Green and Blue Luminescent Carbon Nanodots for Bioimaging Applications, *J. Mater. Chem. B*, 2013, **1**, 5023–5028.

77 S. N. Baker and G. A. Baker, Luminescent Carbon Nanodots: Emergent Nanolights, *Angew. Chem., Int. Ed.*, 2010, **49**, 6726–6744.

78 X. Li, M. Rui, J. Song, Z. Shen and H. Zeng, Carbon and Graphene Quantum Dots for Optoelectronic and Energy Applications: A Review, *Adv. Funct. Mater.*, 2015, **25**, 4929–4947.

79 S. T. Yang, L. Cao, P. G. Luo, F. Lu, X. Wang, H. Wang, M. J. Meziani, Y. Liu, G. Qi and Y. P. Sun, Carbon Dots for Optical Imaging in Vivo, *J. Am. Chem. Soc.*, 2009, **131**, 11308–11309.

80 M. L. Liu, B. B. Chen, C. M. Li and C. Z. Huang, Carbon Dots: Synthesis, Formation Mechanism, Fluorescence Origin and Sensing Applications, *Green Chem.*, 2019, **21**, 449–471.

81 Y. Wang, K. Kalantar-Zadeh, A. Kis, J. N. Coleman and M. S. Strano, Electronics and Optoelectronics of Two-Dimensional Transition Metal Dichalcogenides, *Nat. Nanotechnol.*, 2012, **7**, 699–712.

82 M. Zheng, S. Ruan, S. Liu, T. Sun, D. Qu, H. Zhao, Z. Xie, H. Gao, X. Wang, K. Ge, H. Su, Y. Xiong, Y. Li and J. Tang, Self-Targeting Fluorescent Carbon Dots for Diagnosing and Mapping Hepatocellular Carcinoma, *Nanoscale*, 2019, **11**, 22092–22099.

83 Y. P. Sun, B. Zhou, Y. Lin, W. Wang, K. A. S. Fernando, P. Pathak, M. J. Meziani, B. A. Harruff, X. Wang, H. Wang, P. G. Luo, H. Yang, M. E. Kose, B. Chen, L. M. Veca and S. Y. Xie, Quantum-Sized Carbon Dots for Bright and Colorful Photoluminescence, *J. Am. Chem. Soc.*, 2006, **128**, 7756–7757.

84 A. Cayuela, M. L. Soriano, C. Carrillo-Carrión and M. Valcárcel, Semiconductor and Carbon-Based Fluorescent Nanodots: The Need for Consistency, *Chem. Commun.*, 2016, **52**, 1311–1326.

85 C. Wang, Z. Xu, C. Zhang, Q. Qiao, L. Zhang, R. Zhang, Y. Yu and X. Liu, Highly Efficient and Stable Green-Emitting Carbon Dots for Bioimaging, *Nanoscale*, 2014, **6**, 1775–1781.

86 P. Szmyt, B. Buszewski and R. Gadzała-Kopciuch, *Mater. Chem. Phys.*, 2020, **242**, 122484.

87 R. Atchudan, T. N. J. I. Edison, K. R. Aseer, S. Perumal, N. Karthik and Y. R. Lee, Highly Fluorescent Nitrogen-Doped Carbon Dots Derived from Phyllanthus acidus for Selective Detection of Ferric Ions, *J. Photochem. Photobiol., B*, 2018, **185**, 242–252.

88 D. Sun, T. Liu and C. Wang, *et al.*, Hydrothermal Synthesis of Fluorescent Carbon Dots from Gardenia Fruit for Sensitive onoff-on Detection of Hg^{2+} and Cysteine, *Spectrochim. Acta, Part A*, 2020, **240**, 118598.

89 C. Wang, Y. Wang, H. Shi, Y. Yan, E. Liu, X. Hu and J. Fan, A strong blue fluorescent nanoprobe for highly sensitive and selective detection of mercury(II)based on sulfur doped carbon quantum dots, *Mater. Chem. Phys.*, 2019, 145–151.

90 B. B. Wang, J. Cheng Jin, Z. Qiang Xu, Z. Wen Jiang, X. Li, F. Lei Jiang and F. Liu, Single-step synthesis of highly photoluminescent carbon dots for rapid detection of Hg^{2+} with excellent sensitivity, *J. Colloid Interface Sci.*, 2019, **551**, 101–110.

91 B. S. Onishi, A. N. Carneiro Neto and S. J. Ribeiro, Carbon Dot-LAPONITE® Hybrid Nanocomposites as Selective Turn-Off Sensors for Hg^{2+} Detection and Photoluminescence Quenching Mechanism, *ACS Omega*, 2024, **9**(52), 51204–51212.

 © 2025 The Author(s). Published by the Royal Society of Chemistry